Regulation of landslide motion by dilatancy and pore pressure feedback

Richard M. Iverson
U.S. Geological Survey, Vancouver, Washington, USA

Received 17 November 2004; revised 3 March 2005; accepted 28 March 2005; published 25 June 2005.

[1] A new mathematical model clarifies how diverse styles and rates of landslide motion can result from regulation of Coulomb friction by dilation or contraction of water-saturated basal shear zones. Normalization of the model equations shows that feedback due to coupling between landslide motion, shear zone volume change, and pore pressure change depends on a single dimensionless parameter α, which, in turn, depends on the dilatancy angle ψ and the intrinsic timescales for pore pressure generation and dissipation. If shear zone soil contracts during slope failure, then $\alpha < 0$, and positive pore pressure feedback and runaway acceleration are inevitable. If the shear zone dilates, then $\alpha > 0$, and negative feedback permits slow, steady landslide motion to occur while positive pore pressure is supplied by rain infiltration. Steady state slip velocities v_0 obey $v_0 = -(K/\psi)\, p_e^*$, where K is the hydraulic conductivity and p_e^* is the normalized (dimensionless) negative pore pressure generated by dilation. If rain infiltration and attendant pore pressure growth continue unabated, however, their influence ultimately overwhelms the stabilizing influence of negative p_e^*. Then, unbounded landslide acceleration occurs, accentuated by an instability that develops if ψ diminishes as landslide motion proceeds. Nonetheless, numerical solutions of the model equations show that slow, nearly steady motion of a clay-rich landslide may persist for many months as a result of negative pore pressure feedback that regulates basal Coulomb friction. Similarly stabilized motion is less likely to occur in sand-rich landslides that are characterized by weaker negative feedback.

Citation: Iverson, R. M. (2005), Regulation of landslide motion by dilatancy and pore pressure feedback, *J. Geophys. Res.*, *110*, F02015, doi:10.1029/2004JF000268.

1. Introduction

[2] Landslides exhibit a great diversity of movement styles and rates, ranging from barely discernable creeping slip to catastrophic avalanching. This diversity has large implications for downslope hazards and sediment delivery, but it cannot be assessed using traditional slope stability analyses, which consider only conditions necessary to trigger landsliding. Many assessments of landslide diversity have emphasized the qualitative effects of soil and rock properties as well as geologic, hydrologic, and topographic variables [e.g., *Cruden and Varnes*, 1996]. On the other hand, quantitative models of landslide motion generally have focused on specific types of landslides, such as slow earthflows or rapid debris flows and rock avalanches [e.g., *Vulliet and Hutter*, 1988; *Takahashi*, 1991; *Baum and Johnson*, 1993; *Hungr*, 1995]. No theory has been available to bridge the gap in understanding landslide movement that ranges from a few centimeters per year to many meters per second, and no theory has provided a mechanistic framework for assessing whether slow, persistent movement might eventually lead to catastrophic acceleration.

[3] In this paper I describe a new theoretical model that shows how mechanical feedbacks might be responsible for some of the observed diversity in landslide styles and rates, and might produce abrupt transitions from slow to rapid motion. The model incorporates feedback between landslide displacement and attendant shear zone dilation or contraction that modulates basal pore water pressure and sliding friction. As demonstrated in experiments, shear zone contraction produces elevated pore pressures and positive feedback, whereas shear zone dilation produces diminished pore pressures and negative feedback [e.g., *Iverson et al.*, 2000]. Consequences of this feedback depend on a variety of factors, but in all cases the strength of feedback depends on the shear zone dilatancy and intrinsic timescales for pore pressure generation and dissipation.

[4] The relationship between shear deformation, dilatancy and pore pressure change in granular media has been understood qualitatively since at least the time of *Reynolds* [1885, 1886]. Modern work on dilatancy and pore pressure feedback includes important theoretical contributions by *Frank* [1965], *Rice* [1975], *Rudnicki* [1984], and *Segall and Rice* [1995]. These papers and others aimed principally at understanding fault mechanics emphasize mechanical systems in which near-field deformation and pore pressure obey specified stress-strain formulae and are driven by far-

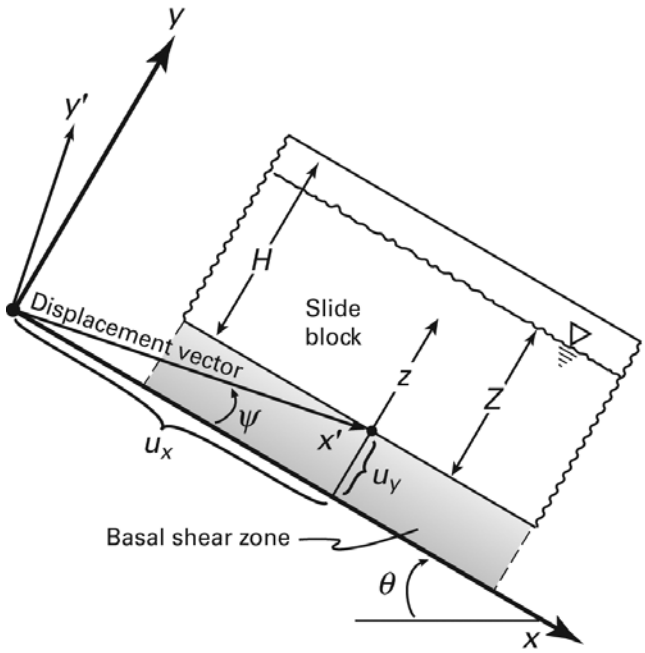

Figure 1. Schematic illustrating the coordinate systems and geometric variables used to analyze slide block motion and pore pressure evolution.

field tectonic strain. The landslide problem has many similarities but differs fundamentally because motion is driven by imposed stress, not strain. In the model developed here, the stress state is treated as one-dimensional and statically determinate, and use of explicit stress-strain formulae is therefore unnecessary. Instead, landslide motion obeys Newton's second law and is resisted only by basal Coulomb friction. This simple model provides a parsimonious framework for evaluating effects of pore pressure feedback, and it also provides a foundation for development and testing of more realistic landslide models that account for multidimensional deformation and internal friction [e.g., *Iverson and Denlinger*, 2001; *Savage and Iverson*, 2003; *Denlinger and Iverson*, 2004].

[5] The model developed here also can be viewed as an extension of *Hutchinson*'s [1986] sliding-consolidation model. In both models rigid body translation of a landslide block is regulated by basal pore fluid pressure that obeys a one-dimensional diffusion (i.e., consolidation) equation. However, pore pressure feedback, which is a central feature of the present model, is absent in the sliding-consolidation model.

2. Model Formulation

[6] The new model has two primary components, an ordinary differential equation describing downslope motion of a slide block that obeys Newton's second law, and a partial differential equation describing diffusion of excess pore fluid pressure generated in a shear zone at the base of the slide block. The differential equations are coupled mathematically through a boundary condition that summarizes the effects of volume change in the basal shear zone. This coupling provides a mechanism for feedback and nonlinear response, and an additional nonlinearity is imposed by the constraint that slide block motion is irreversible (i.e., under no circumstances does the slide block move uphill).

2.1. Equations Governing Slide Block Motion

[7] Consider a solid, poroelastic block descending (or poised to descend) a rigid, planar slope that is inclined at an angle θ and aligned with rectangular Cartesian coordinates x and y (Figure 1). The block is one-dimensional in the sense that internal stresses and strains are assumed to vary only normal to the block surface. However, motion of the block is two-dimensional in the sense that rigid body displacement in the x direction (u_x) is accompanied by rigid body displacement in the y direction (u_y), which results solely from volume change in a plastically deforming shear zone at the base of the block. In other words, rigid body displacement occurs not in the direction of x, but instead in the direction of a rotated coordinate x' (Figure 1).

[8] Specification of the initial volume or porosity of the basal shear zone is unnecessary, but the propensity for shear zone volume change is specified by a dilatancy angle, ψ, which is positive in the case of dilative shearing and negative in the case of contractive shearing. Phenomenologically, ψ can be represented in terms of incremental components of slide block displacement by [cf. *Taylor*, 1948; *Nemat-Nasser*, 1980; *Bolton*, 1986]

$$\tan\psi = \Delta u_y/\Delta u_x. \tag{1a}$$

Experimental data show that values $\psi < 0.35$ (i.e., $\psi < 20°$) are typical of granular soils, such that $\tan\psi \approx \psi$ [*Bolton*, 1986]. Therefore for infinitesimal displacements (1a) can be approximated by

$$\psi = du_y/du_x. \tag{1b}$$

In general, the value of ψ evolves as slide block displacement proceeds, and $\psi \to 0$ if displacements become large enough that the deforming soil in the shear zone approaches a constant, critical state porosity [e.g., *Roscoe*, 1970; *Negussey et al.*, 1988]. Part of the analysis below is aimed at gaining a clear understanding of slide block behavior for simple cases in which ψ is constant, but numerical results are then presented for cases in which ψ decays toward zero as slide block displacement proceeds. Further discussion of the role and evolution of ψ accompanies the presentation of numerical results.

[9] To analyze slide block motion, it is convenient to resolve forces at the base of the block using a coordinate system x'-y' rotated with respect to the x-y system by the angle ψ (Figure 1). Gravity imposes a driving force in the x' direction equal to $\rho gHA \sin(\theta - \psi)$, where H is the slide block thickness, ρ is the slide block mass density averaged over the thickness H, g is the magnitude of gravitational acceleration, and A is the area of the slide block base. The component of gravitational force acting in the y' direction is $-\rho gHA \cos(\theta - \psi)$, and the consequent frictional resistance that opposes motion in the x' direction is $-\rho gHA \cos(\theta - \psi) \tan\phi$, where ϕ is an appropriate basal friction angle. The relationship between ϕ and ψ is discussed in conjunction with equations (4a) and (4b) below.

[10] Basal frictional resistance is modified by basal pore fluid pressure, $p(0, t)$, assumed to act uniformly along the base of the slide block but allowed to vary with time. The component of the fluid pressure force acting in the y' direction reduces the basal frictional force acting in the x' direction by $p(0, t)A \cos\psi \tan\phi$.

[11] Summing the downslope driving force and frictional resisting force yields an expression for the net downslope force in the x' direction,

$$F_{x'} = \rho g H A \sin(\theta - \psi) - \rho g H A \cos(\theta - \psi)\tan\phi + p(0,t)A\cos\psi\tan\phi. \quad (2)$$

If $F_{x'} > 0$, downslope acceleration of the slide block occurs, and the consequent change in momentum in the x' direction is given by $\rho HA(d^2u_{x'}/dt^2) = F_{x'}$. The resultant momentum change in the x direction is smaller by a factor $\cos\psi$, and is given by $\rho HA(d^2u_x/dt^2) = \cos\psi\, F_{x'}$.

[12] Substituting (2) into the expression for the x direction momentum change and dividing the result by ρgHA yields an equation describing the x component of slide block motion:

$$\frac{1}{g}\frac{d^2u_x}{dt^2} = \cos\psi\left[\sin(\theta-\psi) - \left(\cos(\theta-\psi) - \frac{p(0,t)}{\rho g H}\cos\psi\right)\tan\phi\right]. \quad (3a)$$

Through use of trigonometric identities [*Dwight*, 1961, equations (401.02) and (401.03)], (3a) can be rewritten in a form that isolates the influences of θ, ϕ, and ψ:

$$\frac{1}{g}\frac{d^2u_x}{dt^2} = \cos^2\psi\left\{\left[\sin\theta - \left(\cos\theta - \frac{p(0,t)}{\rho g H}\right)\tan\phi\right] - \tan\psi(\cos\theta + \sin\theta\tan\phi)\right\}. \quad (3b)$$

The term in square brackets on the right-hand side of (3b) describes the net x direction force that exists if $\psi = 0$. This term can be generalized to include the effects of cohesive strength c by adding $-c/\rho gH$, but effects of cohesion play no essential role in the problem at hand, and are therefore omitted. Equations (3a) and (3b) can also be generalized to account for centripetal accelerations due to slide block rotation caused by changes in ψ or θ, but for the sake of brevity and clarity, the ensuing analysis neglects effects of rotation.

[13] In this simple model the effect of dilatancy ψ on shear resistance is statically equivalent to a modification of the effective friction angle [cf. *Rowe*, 1962; *Bolton*, 1986; *Negussey et al.*, 1988], and this equivalence can be illustrated by setting the acceleration term on the left-hand side of (3b) to zero. Dividing all terms of the resulting equation by $\cos^2\psi\cos\theta$ yields an equation governing limiting equilibrium of the static slide block:

$$\tan\theta(1 - \tan\phi\tan\psi) - (\tan\phi + \tan\psi) + \frac{p_{\mathrm{crit}}}{\rho g H\cos\theta}\tan\phi = 0, \quad (4a)$$

where p_{crit} is the critical value of the basal pore pressure $p(0, t)$ necessary to trigger motion. Setting $\psi = 0$ reduces (4a) to a form of the standard infinite-slope limit-equilibrium equation [e.g., *Taylor*, 1948], whereas setting $p_{\mathrm{crit}} = 0$ reduces (4a) to the static balance

$$\tan\theta = \tan(\phi + \psi) = \frac{\tan\phi + \tan\psi}{1 - \tan\phi\tan\psi}. \quad (4b)$$

Equation (4b) is analogous to the standard "angle of repose" equation, $\tan\theta = \tan\phi$, but (4b) indicates that the effective basal friction angle resisting motion of the slide block in the x direction is $\phi + \psi$. This result recapitulates findings of *Rowe* [1962] and *Nemat-Nasser* [1980], who analyzed limiting equilibrium of dilatant granular masses subject to specified external forces. The momentum balances used here differ from the static balances considered by *Rowe* [1962] and *Nemat-Nasser* [1980], because here the force components imposed by gravity as well as the resulting acceleration of the slide block can vary as a consequence of the geometrical influence of ψ.

[14] A key point established by (3a), (3b), (4a), and (4b) is that quasistatic effects of shear zone dilatancy ψ can be regarded as modifications of either the effective slope angle or the effective friction angle. However, the friction angle ϕ employed in this paper is independent of ψ and does not depend on volume changes associated with shear zone dilation and contraction [cf. *Negussey et al.*, 1988].

2.2. Equations Governing Pore Pressure Diffusion

[15] To analyze evolution of pore fluid pressure, it is convenient to use a coordinate z that translates with the base of the slide block (Figure 1). The coordinate

$$z = y - u_y \quad (5)$$

specifies that the base of the slide block (i.e., the upper margin of the basal shear zone) is located at $z = 0$ at all times.

[16] A water table is assumed to exist a priori at height $z = Z$ above the base of the slide block (Figure 1), and evolution of the pore pressure p beneath the water table is assumed to be governed by the conventional linear diffusion equation that describes transient, one-dimensional, saturated groundwater flow in a poroelastic medium that undergoes no change in total stress:

$$\frac{\partial p}{\partial t} = D\frac{\partial^2 p}{\partial z^2}. \quad (6)$$

Here D is the hydraulic diffusivity (also known as the consolidation coefficient), which is assumed to be constant. Equation (6) is readily derived using the principles of mass conservation, Darcian flux of pore water, effective stress, and one-dimensional elastic deformation [e.g., *Terzaghi*, 1943; *Gambolati*, 1973], but the derivation is omitted here for the sake of brevity. A more realistic pressure-diffusion model would account for evolution of D due to changes in material properties or water content, but a need exists to understand the behavior of a simple model with a constant D before this complication is addressed.

[17] For purposes of the analysis below, it is useful to split the total pore pressure p in (6) into two components:

$$p(z,t) = p_i(z,t) + p_e(z,t), \quad (7)$$

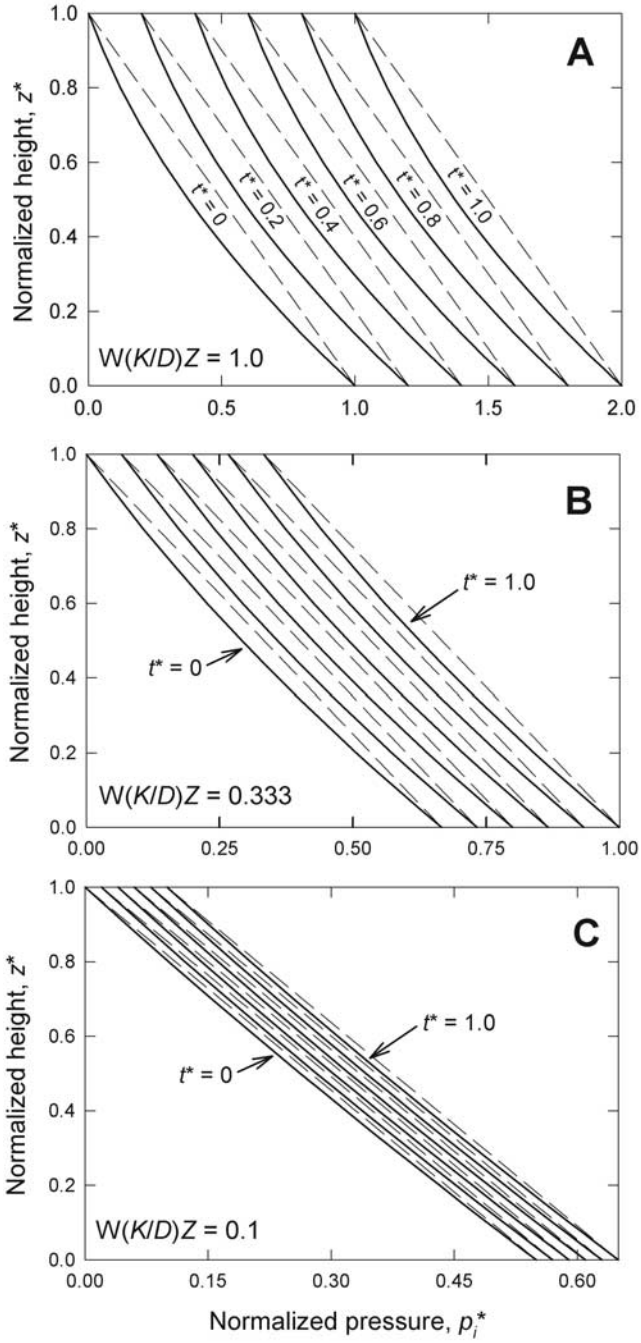

Figure 2. Graphs depicting evolution of the imposed pore pressure distribution, which is described in detail in Appendix A. Solid lines represent equation (12), and dashed lines represent a linear approximation of (12). All graphs depict behavior for the same normalized time sequence from $t^* = 0$ to $t^* = 1$, but Figures 2a, 2b, and 2c show behavior for differing values of the parameter $W(K/D)Z$. All graphs assume $\beta = 0.5$.

where p_i is the imposed pore pressure due to processes such as rain infiltration, and p_e is the excess pore pressure (either positive or negative) that develops in response to contraction or dilation of the basal shear zone. Substitution of (7) into (6) yields a diffusion equation for coevolution of the two pressure components p_e and p_i.

2.2.1. Imposed Pore Pressure

[18] Evolution of the imposed pressure p_i serves to trigger slide block motion and also influences postfailure sliding, but in the model developed here, this behavior merely provides a backdrop for assessing the effects of feedback involving coupled slide block motion and excess pore pressure production. Therefore to facilitate analysis of feedback, p_i is specified so that it has a simple mathematical form that emulates pore pressure distributions beneath a rising water table, without representing the complicated dynamics of water table accretion. Thus p_i is specified by

$$p_i(z,t) = \rho_w g\left[\beta(Z-z) + WK\left(t + \frac{(Z-z)^2}{2D}\right)\right], \qquad (8)$$

where ρ_w is the pore water density, K is the saturated hydraulic conductivity beneath the water table, and β and W are dimensionless constants of order 1.

[19] Appendix A provides an in depth discussion of β, W and the form of equation (8), but a few key properties of the equation deserve mention here. First, (8) satisfies a diffusion equation, such that beneath the water table one-dimensional groundwater flow caused by rain infiltration obeys [cf. *Iverson*, 2000]

$$\frac{\partial p_i}{\partial t} = D\frac{\partial^2 p_i}{\partial z^2}. \qquad (9)$$

Second, (8) satisfies flux (i.e., pressure gradient) boundary conditions given by

$$\frac{\partial p_i}{\partial z}(Z,t) = -\rho_w g\beta \qquad (10)$$

$$\frac{\partial p_i}{\partial z}(0,t) = -\rho_w g\left(\beta + W\frac{K}{D}Z\right). \qquad (11)$$

These conditions imply that the downward flux of water at height $z = Z$ exceeds that at the slide block base at $z = 0$. The consequent flux imbalance serves to increase the pore pressure between $z = Z$ and $z = 0$, and the rate of increase depends on $W(K/D)Z$, a dimensionless quantity that summarizes the effect of transient rain infiltration on groundwater storage beneath the water table (Appendix A). Effects of the groundwater flux imbalance are depicted graphically in Figure 2, which shows plots of a normalized version of (8):

$$p_i^*(z^*,t^*) = \beta(1-z^*) + W\frac{K}{D}Z\left\{t^* + \frac{1}{2}[1 - z^* - z^*(1-z^*)]\right\}. \qquad (12)$$

Here $p_i^* = p_i/\rho_w gZ$ is the normalized pore pressure, $z^* = z/Z$ is the normalized height, and $t^* = t/(Z^2/D)$ is the normalized time. The graphs of Figure 2 show that as values of $W(K/D)Z$ decline toward a limit of zero, pore pressure distributions described by (8) and (12) converge toward steady state (i.e., linear) distributions.

[20] Equation (8) implies that the imposed pore pressure at the slide block base obeys

$$p_i(0,t) = \rho_w g\left[\beta Z + WK\left(t + Z^2/2D\right)\right], \qquad (13)$$

which indicates a linear increase of pressure with time (Figure 2). Once slide block motion commences, excess basal pore pressure that develops in response to motion is added to (13) to determine the total basal pore pressure that affects the slide block's basal friction.

2.2.2. Excess Pore Pressure

[21] Because evolution of the total pore pressure $p_i + p_e$ is governed by a diffusion equation, and p_i satisfies its own diffusion equation, the excess pore pressure p_e also satisfies a diffusion equation:

$$\frac{\partial p_e}{\partial t} = D\frac{\partial^2 p_e}{\partial z^2}. \tag{14}$$

This is the standard equation used to assess evolution of excess pore pressure in soils without changes in total stress [e.g., *Lambe and Whitman*, 1979]. In the present instance, however, the implications of (14) are nonstandard because generation of excess pore pressure in the basal shear zone couples (14) to slide block motion.

[22] Coupling of (14) to slide block motion is specified by a basal boundary condition that describes pore fluid exchange between the deforming basal shear zone and the overlying slide block. If the solid and fluid constituents in the shear zone are effectively incompressible (a reasonable assumption for the total stress magnitudes <1 MPa typical of most landslides), porosity change within the shear zone determines the fluid influx or efflux that accompanies shear zone volume change. Assuming that this fluid flux obeys Darcy's law, the excess pore pressure gradient that develops in reaction to the flux through the boundary of the shear zone is given by [*Iverson*, 1993]

$$\frac{\partial p_e}{\partial z}(0,t) = \frac{\rho_w g}{K}\frac{du_y}{dt}. \tag{15a}$$

Here du_y/dt is the slope-normal velocity component of the slide block, which is directly proportional to the rate of shear zone volume change. The derivation of (15a) assumes that fluid flow associated with $\partial p_e/\partial z(0, t)$ occurs only through the upper surface of the basal shear zone, but this assumption can easily be modified if desired [*Iverson*, 1993].

[23] The basal boundary condition (15a) can be expressed in alternative forms. For example, (15a) can be expressed in terms of the downslope slide block velocity $v = du_x/dt$ because (1b) implies that $du_y/dt = \psi\,(du_x/dt)$. Thus (15a) may be rewritten as

$$\frac{\partial p_e}{\partial z}(0,t) = \frac{\rho_w g}{K}\psi v. \tag{15b}$$

A more complicated form of the basal boundary condition applies to the total pore pressure gradient $\partial p/\partial z$, and this form is obtained by adding (15a) or (15b) to the imposed basal pressure gradient specified by (11).

[24] The upper boundary condition stipulates that $p_e = 0$ at the water table. However, because the evolving position of the water table may not be precisely known, the boundary condition is enforced at the original water table position $z = Z$:

$$p_e(Z,t) = 0. \tag{16}$$

Equation (16) applies exactly for the initial condition, which stipulates that no excess pore pressure exists:

$$p_e(z,0) = 0. \tag{17}$$

Equation (16) also applies exactly for steady state conditions in which negative excess pore pressure combines with the imposed pore pressure to hold the total pore pressure, downward water flux, and water table height constant. (Development of such steady states is detailed in section 3 below.) For unsteady states with evolving water table heights, the maximum error that results from use of (16) can be estimated by considering a case in which the water table height is unregulated by excess pore pressure feedback and therefore grows at the rate WK implied by (8). In this case (16) is replaced by the boundary condition $p_e(Z + WKt,t) = 0$. Numerical trials showed little sensitivity to the use of this condition versus the simpler condition given by (16). Therefore (16) is adopted as a satisfactory upper boundary condition.

2.3. Normalized Equations

[25] The equations described above are normalized and simplified by introducing dimensionless variables defined as

$$z^* = \frac{z}{Z}, \quad t^* = \frac{t}{Z^2/D}, \quad v^* = \frac{du_x/dt}{g(Z^2/D)}, \quad p_e^* = \frac{p_e}{\rho_w g Z}, \quad p_i^* = \frac{p_i}{\rho_w g Z}. \tag{18}$$

Also, to simplify notation, two groups of geometric parameters in (3a) are renamed as

$$C_1 = \cos\psi\sin(\theta - \psi) \tag{19}$$

$$C_2 = \cos\psi\cos(\theta - \psi), \tag{20}$$

and a parameter that encapsulates the effects of the density ratio ρ_w/ρ and length-scale ratio Z/H is defined as

$$C_3 = \cos^2\psi\frac{\rho_w}{\rho}\frac{Z}{H}. \tag{21}$$

The primary length scale is chosen to be Z rather than H because use of Z minimizes the appearance of parameters in the normalized equations. However, use of H is a reasonable alternative, and the choice of length scale does not influence the physically relevant results. For similar reasons, Z^2/D is chosen as the sole timescale in the normalized equations, although the analysis below shows that another timescale is also important.

[26] Combining (18), (19), (20), and (21) with (3), (6), (7), (8), (9), (15b) and (16) yields a system of normalized governing equations and boundary conditions

$$\frac{dv^*}{dt^*} = C_1 - [C_2 - C_3(p_i^*(0,t^*)) + p_e^*(0,t^*)]\tan\phi, \tag{22}$$

$$\frac{\partial p_e^*}{\partial t^*} = \frac{\partial^2 p_e^*}{\partial z^{*2}}, \tag{23}$$

$$\frac{\partial p_e^*}{\partial z^*}(0,t^*) = \alpha v^*, \tag{24}$$

$$p_e^*(1,t^*) = 0, \tag{25}$$

Table 1. Parameter Values Used in Computations[a]

Parameter and Units	Experimental Landslide Loose Loamy Sand	Experimental Landslide Dense Loamy Sand	Minor Creek Landslide Gravelly Sandy Clay
D, m^2/s	1×10^{-3}	3×10^{-3}	1×10^{-6}
g, m/s^2	9.8	9.8	9.8
H, m	0.65	0.65	6.0
K, m/s	2×10^{-4}	2×10^{-5}	5×10^{-8}
v_0, m/s	0	0	0
W, dimensionless	1	1	1
Z, m	0.65	0.46, 0.65	5.6
α, dimensionless	0, -2.2×10^6	3.6×10^6, 7.2×10^6	3.2×10^{14}
β, dimensionless	0	0	0
θ, deg	31	31	15
ρ, kg/m^3	1800	2000	2200
ρ_w, kg/m^3	1000	1000	1000
ϕ, deg	35	35	15
ψ, deg	0, -6	6	3

[a]Data sources are *Iverson* [1984], *Iverson and Major* [1987], *Hovind* [1990], and *Iverson et al.* [2000]. Where two values are tabulated, they apply to two different scenarios described in the text.

in which the dependent variables are the normalized downslope slide block velocity v^* and the normalized excess pore pressure p_e^*. Accompanying initial conditions are

$$v^*(0) = v_0^* \tag{26}$$

$$p_e^*(z^*, 0) = 0, \tag{27}$$

where v^*_0 is a specified initial velocity, commonly equal to zero.

[27] Equations (22)–(27) show that only a few parameters affect the coupled evolution of v^* and p_e^*, and of these parameters only α varies greatly. (The other parameters are the geometric quantities C_1, $C_2 \tan\phi$, and $C_3 \tan\phi$, which are unlikely to have values outside the range 0.1–1.) The parameter α appears in the basal boundary condition (24) and is defined by

$$\alpha = \left[\frac{Z^2/D}{K/g}\right]\psi. \tag{28}$$

Physical interpretation of α is straightforward. The sign of α is determined by the sign of the dilatancy angle ψ, such that $\alpha > 0$ for dilatant shearing and $\alpha < 0$ for contractive shearing. The magnitude of α varies in proportion to the term in brackets in (28). The denominator of this term is the timescale for pore pressure generation due to gravity-driven deformation of the basal shear zone, and the numerator is the timescale for pore pressure diffusion within the slide block. Together with ψ, the ratio of these two timescales controls the strength of coupling of the differential equations (22) and (23). Typically $|\alpha| \gg 1$ because $(Z^2/D)/(K/g) > 1000$ is typical of most landslides (e.g., Table 1). Therefore effects of feedback on coupled solutions of (22) and (23) are generally strong.

3. Analytical Results

[28] Although numerical methods are generally needed to solve the coupled system of time-dependent equations (22)–(27), the analysis below provides physical insight by using exact solutions to assess the existence of steady states and their stability when subjected to transient perturbations.

3.1. Steady States

[29] Steady sliding occurs if the right-hand side of the equation of motion (22) equals zero. This condition exists if the total basal pore pressure $p_i^*(0, t^*) + p_e^*(0, t^*)$ has a critical value given by

$$p_{\text{crit}}^* = \frac{1}{C_3}\left[C_2 - \frac{C_1}{\tan\phi}\right], \tag{29}$$

where $p_{\text{crit}}^* = p_{\text{crit}}/\rho_w g Z$ is the normalized version of the total basal pore pressure necessary to balance forces (see equation (4a)). A special steady state exists when forces are statically balanced at limiting equilibrium.

[30] Through use of p_{crit}^*, the equation of motion (22) can be rewritten as

$$\frac{1}{C_3 \tan\phi}\frac{dv^*}{dt^*} = p_i^*(0, t^*) + p_e^*(0, t^*) - p_{\text{crit}}^*. \tag{30}$$

The steady state solution of (30) is $v^* = v_0^*$, and the static solution $v^* = 0$ represents a special steady state.

[31] The excess pore pressure equation (23) has a steady state solution that satisfies the basal and upper boundary conditions (24) and (25). This solution,

$$p_e^*(z^*) = -\alpha v_0^*(1 - z^*), \tag{31}$$

implies that an infinite number of steady states can exist, and that each steady pore pressure distribution is associated with a particular value of the steady sliding velocity, given by

$$v_0^* = -\frac{1}{\alpha}p_e^*(0) = \frac{1}{\alpha}[p_i^*(0) - p_{\text{crit}}^*]. \tag{32a}$$

At steady state, the vertical profiles of the imposed, excess, and total pore pressures are all linear, and the downward flux of water across the water table equals the downward flux into the dilating basal shear zone. The steady sliding rate v^*_0 increases in direct proportion to this water flux.

[32] The physical implications of (32a) can be further illustrated by writing the equation in terms of dimensional variables:

$$v_0 = -\frac{K}{\psi}\left[\frac{p_e(0)}{\rho_w g Z}\right] = \frac{K}{\psi}\left[\frac{p_i(0) - p_{\text{crit}}}{\rho_w g Z}\right]. \tag{32b}$$

This form of the equation shows that steady sliding velocities v_0 are likely to be no larger than K/ψ, as the pore pressure factor in brackets on the right-hand side of the equation is unlikely to be larger than 1. Thus K/ψ may be interpreted as an "intrinsic" scale for the steady state slide block velocity, and this scale is smaller by a factor α than the "extrinsic" velocity scale $g(Z^2/D)$ used in the unsteady velocity equation (22).

[33] Figure 3 depicts graphs of (32b) that illustrate how the steady slide block velocity depends on K/ψ and the pore pressure difference $p_i - p_{\text{crit}}$. The behavior shown in Figure 3 superficially mimics the behavior of a viscoplastic (i.e., Bingham) material. That is, slide velocity is proportional to the difference between an imposed net driving force (proportional to $p_i - p_{\text{crit}}$ in this instance) and a threshold necessary to instigate motion (represented by p_{crit} in this instance). This superficial resemblance to viscoplastic behavior exists despite the fact that sliding resistance is provided by rate-independent Coulomb friction. The apparent "viscosity" regulating slide block motion is produced by steady diffusion of excess pore pressure, which can persist only as long as steady dilation persists and the coupling between slide block motion and excess pore pressure production generates steady negative feedback that stabilizes the motion. Analysis of slide block responses to transient perturbations helps clarify the propensity for this type of regulation in more realistic (unsteady state) situations.

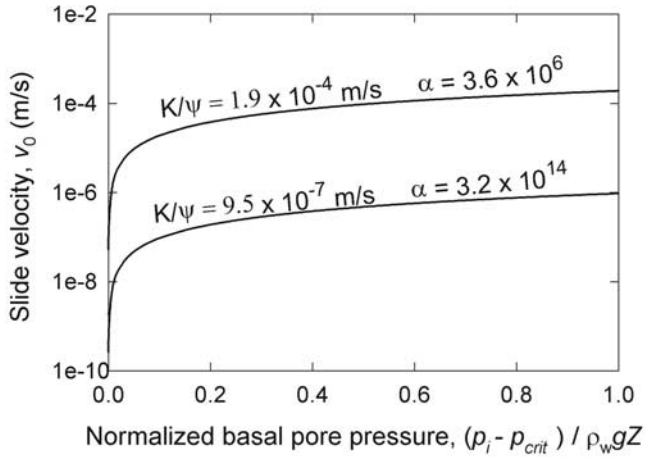

Figure 3. Graphs of steady sliding velocities specified by equation (32b). Velocities are graphed as functions of the normalized value of the net basal pore pressure $p_i - p_{\text{crit}} = -p_e$. The graphs employ values of K/ψ and α for dilative landslide soil, with physical properties summarized in Table 1.

3.2. Transient Perturbations

[34] To facilitate analysis of transient responses, it is useful to couch the slide block equation of motion (30) in terms of new variables. A rescaled slide block velocity is defined as

$$\tilde{v}^* = v^*/C_3 \tan\phi. \tag{33}$$

The rescaled velocity, imposed basal pore pressure, and excess basal pore pressure are then decomposed into steady components (denoted by a subscript s) and transient components (denoted by a prime):

$$\begin{gathered}\tilde{v}^* = \tilde{v}_s^* + \tilde{v}^{*\prime}(t^*), \quad p_e^*(0,t^*) = p_e^*|_s + p_e^{*\prime}(t^*), \\ p_i^*(0,t^*) = p_i^*|_s + p_i^{*\prime}(t^*).\end{gathered} \tag{34}$$

In the remainder of this section, asterisks are omitted to simplify the notation, but the variables are normalized as described above.

[35] Substitution of (33) and (34) into (30) and cancellation of steady state terms that sum to zero yields an equation of motion obeyed by the transient components

$$\frac{d\tilde{v}'}{dt} = p_e'(t) + p_i'(t). \tag{35}$$

If $\tilde{v}'$ and p_e' represent arbitrarily small perturbations or deviations from a steady state, the dependence of $p_e'(t^*)$ on $\tilde{v}'$ can be approximated by the first term of a Taylor's series expansion, which gives the linear equation

$$p_e'(t) \approx \tilde{v}'\left[\frac{dp_e'}{d\tilde{v}'}\right]_s = \tilde{v}'\frac{dp_e}{dv_0} = -\tilde{v}'\alpha. \tag{36}$$

In (36) the subscript s indicates that the derivative is evaluated about the steady datum state, where perturbations vanish. Equation (32a) thus implies the relation $dp_e/dv_0 = -\alpha$ used in (36).

[36] Substitution of (36) into (35) yields an uncoupled linear differential equation that includes the first-order effects of pore pressure feedback:

$$\frac{d\tilde{v}'}{dt} + \alpha\tilde{v}' = p_i'(t). \tag{37}$$

This equation can be solved for any imposed pore pressure history $p_i'(t)$ by using an integrating factor $e^{\alpha t}$, as described by *Rainville and Bedient* [1974, pp. 37–39]. The solution satisfying the initial condition $\tilde{v}'(0) = \tilde{v}_0$ may be written as

$$\tilde{v}'(t) = e^{-\alpha t}\left[\tilde{v}_0 + \int e^{\alpha t} p_i'(t)dt\right]. \tag{38}$$

[37] The solution (38) behaves differently depending on whether the shear zone soil is contractive ($\alpha < 0$) or dilative ($\alpha > 0$). For $\alpha < 0$ (38) indicates that responses to positive imposed pore pressure perturbations $p_i'(t)$ are necessarily unstable, because $\tilde{v}'(t)$ grows unbounded like $e^{-\alpha t}$. This mathematical instability results from the positive feedback associated with shear zone contraction. Slide block motion produces positive excess pore pressure, which prompts faster slide block motion, which produces more excess pore pressure, and so on. For $\alpha > 0$ slide block responses are

Table 2. Solutions for Slide Block Motion Obtained by Evaluating the Integral in Equation (38) for Various Imposed Pore Pressure Perturbations $p_i(t)$[a]

$p_i'(t)$	$\tilde{v}'(t)$	Comments
W	$\tilde{v}_0\, e^{-\alpha t} + \frac{W}{\alpha}(1 - e^{-\alpha t})$	motion decays to a new steady state with velocity $\tilde{v}_0 + (W/\alpha)$
$We^{-\lambda t}$	$\tilde{v}_0 e^{-\alpha t} + \frac{W}{\alpha-\lambda}(e^{-\lambda t} - e^{-\alpha t})$	motion decays to original steady state with velocity $\tilde{v}_0$
$W(1 - e^{-\lambda t})$	$\tilde{v}_0 e^{-\alpha t} + \frac{W}{\alpha}(1 - e^{-\alpha t}) - \frac{W}{\alpha-\lambda}(e^{-\lambda t} - e^{-\alpha t})$	motion decays to a new steady state with velocity $\tilde{v}_0 + (W/\alpha)$

[a]All solutions assume W and λ are arbitrary constants.

stable because $\tilde{v}'(t)$ decays with time like $e^{-\alpha t}$. Table 2 lists examples of solutions obtained by evaluating the integral in (38) for various imposed pressure perturbations $p'_i(t)$ with limited amplitudes and durations. For $\alpha > 0$ these solutions indicate that the slide block velocity decays to a steady state as time proceeds because dilatancy produces negative pore pressure feedback that stabilizes the motion.

[38] A different type of behavior is possible if $\alpha > 0$ but the imposed basal pore pressure grows continually in time, as described by (13). The normalized version of (13) is

$$p_i(0,t) = \beta + W\frac{K}{D}Z\left(t + \frac{1}{2}\right), \tag{39}$$

which consists of a constant term plus a term that grows linearly with time, $W(K/D)Zt$. Retaining only the time-dependent term in (39), substituting it in (38), and evaluating the resulting integral yields the solution

$$\tilde{v}'(t) = \tilde{v}_0 e^{-\alpha t} + W\frac{K}{D}Z\left(\frac{1}{\alpha}\right)\left[\frac{1}{\alpha}(e^{-\alpha t} - 1) + t\right]. \tag{40}$$

The first term on the right-hand side of (40) represents the decaying influence of the initial condition, whereas the second term represents an evolving competition between accelerating slide block motion described by $(1/\alpha)$ $[W(K/D)Z]t$ and suppression of slide block motion by an amount $(1/\alpha^2)$ $[W(K/D)Z]$ $(e^{-\alpha t} - 1)$. Suppression of motion is significant at short times but decays as time proceeds. This effect is illustrated in Figure 4, in which graphs of (40) show that rapid acceleration is delayed for a time proportional to α. The period of slow, stabilized motion following slope failure can be very long if α is very large, but it eventually gives way to unbounded acceleration. This behavior indicates that shear zone dilation cannot stabilize motion indefinitely if continual forcing by rainfall infiltration occurs, even if the dilatancy angle ψ remains constant.

4. Numerical Results

[39] Numerical methods are used to solve the full system of equations (22)–(27) with unrestricted feedback between the dependent variables v^* and p_e^* and with evolution of ψ. The numerical solution technique is straightforward and employs a stepwise analytical method for (22) and the Crank-Nicolson method for (23) [*Crank*, 1975; *Press et al.*, 1986]. At each time step (22) is solved analytically using pore pressure values from the preceding time step. New pore pressures are then computed by solving (23) with the boundary condition (24) updated to reflect the new slide block velocity. This method can be refined with a predictor-corrector procedure in which updated pore pressures are used to re-solve (22) for the preceding time step, and then an average of the two solutions of (22) is used to re-solve (23) before proceeding. However, trial calculations showed that implementation of this procedure had little effect on results. Therefore the results shown here were generated using a forward time-stepping procedure.

[40] Discretization of (22) and (23) involves several considerations. Because (22) is a first-order, linear equation with coefficients that are constant except for the dependence on pore pressure, a stepwise exact solution of (22) may be written in terms of dimensional variables as

$$\Delta u_x = \frac{1}{2}g(\Delta t)^2\left[C_1 - \left(C_2 - C_3\frac{p_i(0,t) + p_e(0,t)}{\rho_w g Z}\right)\tan\phi\right] + v_{\text{old}}\Delta t + u_{\text{old}}, \tag{41}$$

where Δu_x is the downslope displacement during the time step Δt, and v_{old} and u_{old} are the slide block velocity and displacement at the end of the preceding time step. The accuracy of this solution is limited only by resolution of the basal pore pressure, and accurate resolution of p_e $(0, t)$ requires use of much finer time discretization than would be required for numerical solution of the diffusion equation (22) alone. As a consequence, time steps (Δt) used in all calculations were no larger than 0.1 s, and for short-term calculations were as small as 0.0001 s. Relatively fine spatial discretization of the diffusion equation was also necessary, because accurate resolution of the basal pore pressure gradient that appears in the coupling equation (24)

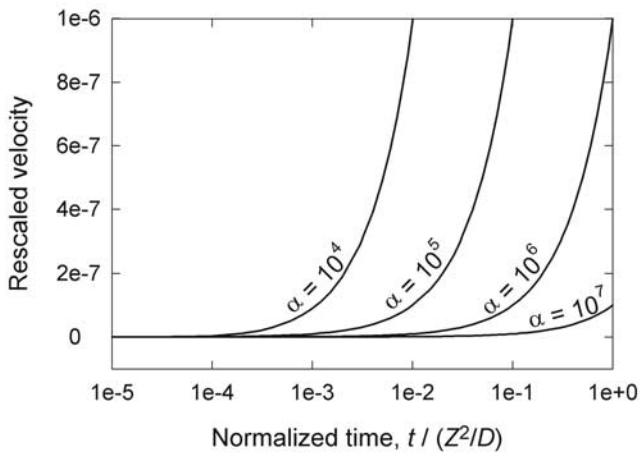

Figure 4. Graph of equation (40) illustrating evolution of the rescaled slide block velocity $\tilde{v}'$ for several values of the parameter α. All graphs employ the initial condition $\tilde{v}'_0 = 0$ and the pore pressure forcing parameter $W(K/D)Z = 1$.

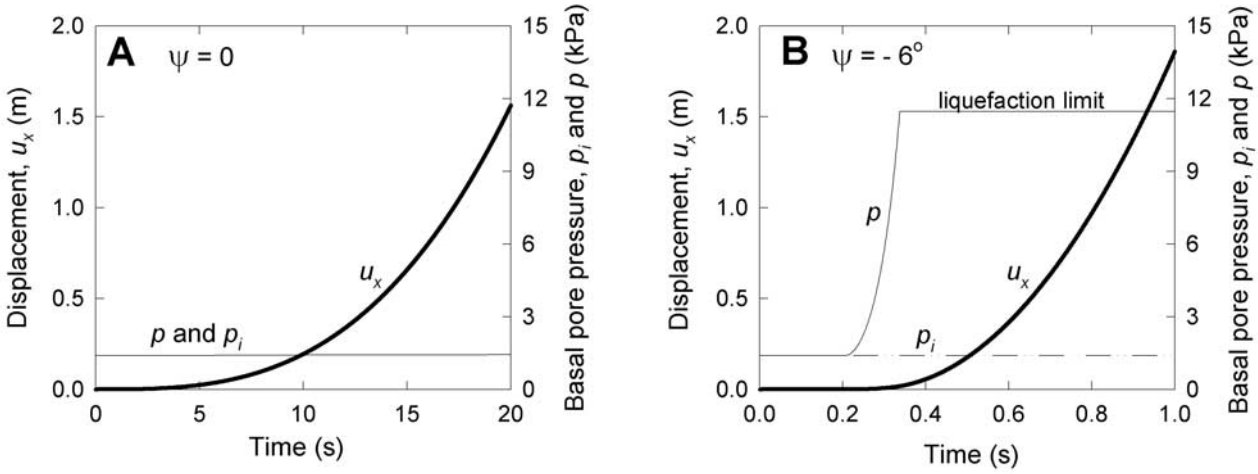

Figure 5. Graphs illustrating evolution of displacement and basal pore pressure computed using parameter values appropriate for an experimental landslide composed of loose loamy sand [*Iverson et al.*, 2000]. Parameter values are listed in Table 1. (a) Behavior with dilatancy angle $\psi = 0$. (b) Behavior with dilatancy angle $\psi = -6°$.

is crucial. Therefore all calculations used a minimum of 50 space nodes to define Δz, and some calculations used as many as 400 space nodes. A final numerical consideration involved the relative sizes of Δt and Δz. Despite the unconditional stability of the Crank-Nicolson method, Courant numbers, defined as $2D(\Delta t)/(\Delta z^2)$, were restricted to be no larger than 1 to promote accurate convergence [cf. *Press et al.*, 1986; *LeVeque*, 2002]. Sizes of time steps were reduced as necessary to satisfy this Courant condition. Despite these restrictions, no computations described here required more than about 10 min of CPU time to execute a double precision FORTRAN program on a personal computer with a 2.3 GHz processor.

[41] The computational results summarized below illustrate landslide behavior in diverse scenarios with and without evolution of the dilatancy angle ψ. For cases in which dilatancy evolves, it is assumed to decay exponentially and obey

$$\psi = \psi_0 \exp[-0.693(u_x/u_{x\,\mathrm{ref}})]. \quad (42)$$

The factor $-0.693 = \ln(1/2)$ is included as a convenience in (42) to make ψ decay to half its initial value ψ_0 when slide block displacement equals the reference value $u_{x\ \mathrm{ref}}$. Appropriate values of $u_{x\ \mathrm{ref}}$ for landslides are not well constrained, but data from laboratory ring shear tests with landslide soil specimens 7 cm thick imply values $u_{x\ \mathrm{ref}} \sim 0.1$ m [e.g., *Iverson et al.*, 2000]. Larger values of $u_{x\ \mathrm{ref}}$ are probably applicable if shear deformation is accommodated in thicker zones, because evolution of dilatancy depends on shear strain, and the average shear strain equals u_x divided by the shear zone thickness. Owing to uncertainty about shear zone thicknesses, shear strains, and the rate of dilatancy decay, computational results are presented for landslides with assumed $u_{x\ \mathrm{ref}}$ values ranging from 0.1 to 10 m.

[42] Table 1 lists the other parameter values used in the computations. The values are appropriate for contractive and dilative sand-rich experimental landslides described by *Iverson et al.* [2000] and for the intensively monitored, clay-rich Minor Creek landslide in northwestern California [*Iverson*, 1984, 1986a, 1986b, 1986c; *Iverson and Major*, 1987; *Hovind*, 1990]. The tabulated ϕ values apply for critical state conditions in which $\psi = 0$ (although the effective basal friction angle consists of the sum of ϕ and ψ, as described in section 2.1). For cases in which ψ decays (and therefore α decays), the tabulated ψ and α represent initial values.

[43] Computational results for all scenarios are shown in graphs (Figures 5–9) that depict coupled evolution of slide block displacement u_x and the imposed and total basal pore pressures, p_i and p. The excess basal pore pressure p_e is not graphed explicitly because it commonly has values <0; however, p_e is easily inferred from the graphs through the relation $p_e = p - p_i$. Computations used to generate all but one graph (Figure 9) used the initial condition $p = p_i = p_{\mathrm{crit}}$ at $t = 0$. Therefore slide block motion commences at the origin of each graph, although the first stages of motion are generally not discernable because the net driving force is initially minuscule.

4.1. Loamy Sand Landslide With Contractive Soil

[44] The computational results depicted in Figure 5 illustrate how contraction of basal shear zone soil produces runaway instability and rapid acceleration during slope failure, corroborating inferences from equation (38). Figure 5a depicts baseline behavior in the absence of shear zone volume change, and Figure 5b depicts behavior when the shear zone contracts with a dilatancy angle $\psi = -6°$. All other parameters used to generate the two panels are fixed and are listed in Table 1. For simplicity the water table height Z is set equal to the slide block thickness H, but results are quite insensitive to alternative values of Z specified within reasonable bounds, as explained in section 4.2.

[45] Figures 5a and 5b show pronounced differences in both the evolution of basal pore pressure and the rate of slide block acceleration. (Note the 20-fold difference in timescales of Figures 5a and 5b.) Without shear zone contraction and pore pressure feedback, acceleration occurs gradually owing to a net driving force that scarcely exceeds the limit equilibrium value 0, and the total basal pore

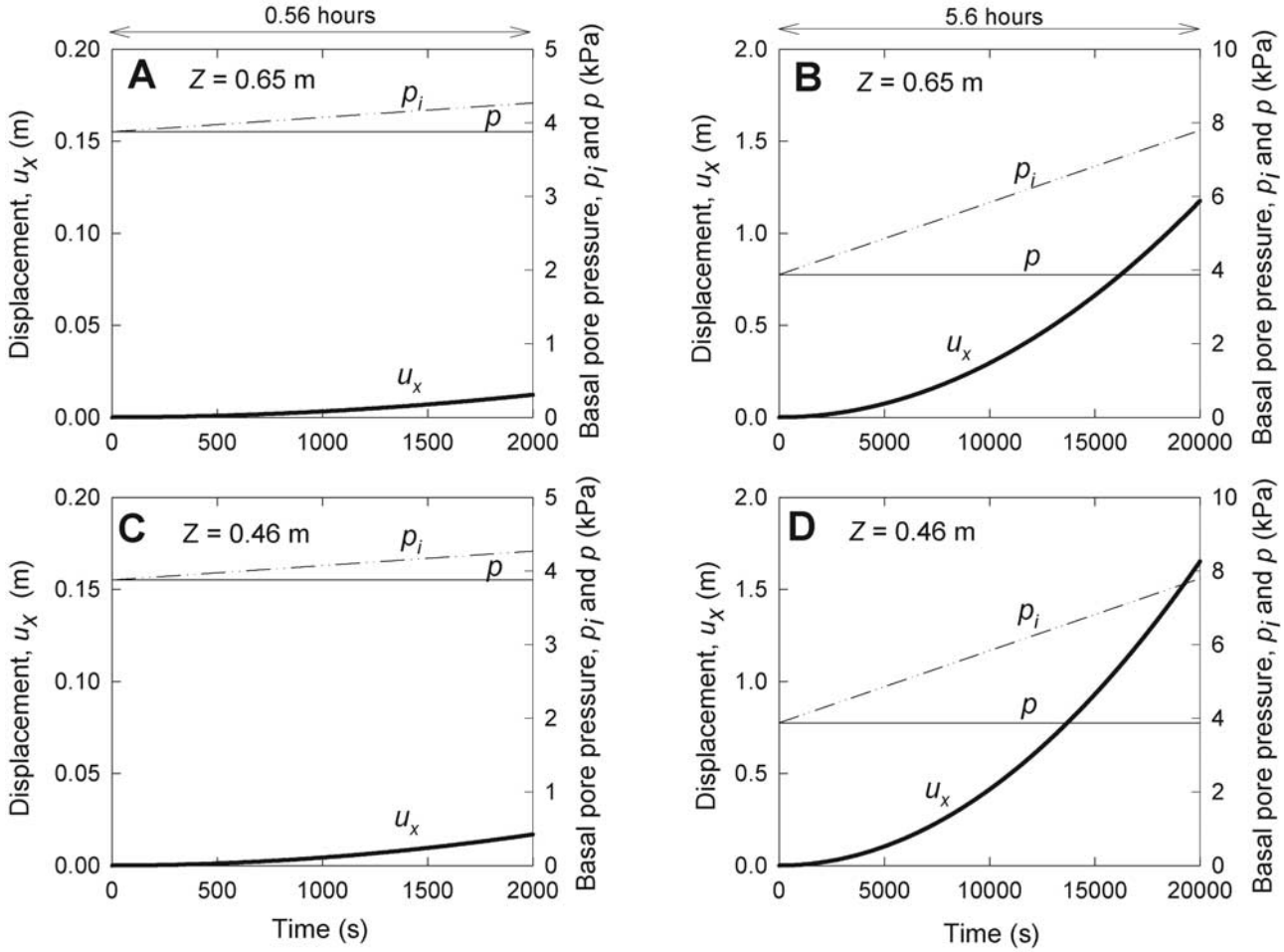

Figure 6. Graphs illustrating the influence of water table height Z on evolution of slide block displacement and basal pore pressure computed using parameter values appropriate for an experimental landslide composed of dense loamy sand [*Iverson et al.*, 2000]. Parameter values are listed in Table 1. Excess basal pore pressure is represented graphically by $p_e = p - p_i$. (a, c) Short-term behavior. (b, d) Long-term behavior.

pressure remains equal to the imposed pressure (Figure 5a). With shear zone contraction, slide block acceleration is increased roughly 20-fold as a consequence of positive pore pressure feedback that causes basal pressure to increase dramatically after failure commences (Figure 5b). Basal pore pressure is subsequently capped at a ''liquefaction limit'' in which basal effective normal stress and Coulomb friction vanish. The rapid acceleration and pore pressure change shown in Figure 5b mimic behavior observed in landslide experiments with contractive sandy soil [*Iverson et al.*, 1997, 2000].

[46] A significant detail in Figure 5b involves the timing of the pore pressure increase that results from shear zone contraction. To avoid production of excess basal pore pressure when displacements are too small to generate much contraction, ψ is held at zero until the displacement reaches $u_x = 0.1$ mm. Displacements of this magnitude occur at $t \sim 0.207$ s, and pore pressure increase occurs rapidly thereafter.

4.2. Loamy Sand Landslide With Dilative Soil

[47] Figures 6 and 7 depict computational results for a scenario similar to that considered in section 4.1, except that the soil is dense and dilative rather than loose and contractive [cf. *Iverson et al.*, 2000]. Table 1 lists parameter values used in the computations. Cases in which the dilatancy angle ψ is constant (Figure 6) and decaying (Figure 7) are considered.

[48] Figure 6 depicts short-term and long-term behavior when ψ is fixed at 6° but values of the water table height Z differ. The maximum value of Z is the slide block thickness H, and the minimum value of Z is constrained by the fact that the initial imposed basal pore pressure must equal the pressure p_{crit} necessary to trigger motion. Provided that the downward groundwater flux q_z is zero or positive, the minimum water table height is given by $Z_{min} = p_{crit}/(\rho_w g \cos \theta)$, which applies for slope-parallel groundwater flow [cf. *Iverson*, 1991]. Figure 6 shows that the effects of Z within the range $Z_{min} \leq Z \leq H$ are quite modest.

[49] Figure 6 shows slide block accelerations roughly 0.01 times as large as in a comparable case without dilation (Figure 5a), and shows that the total basal pore pressure p remains close to the limit equilibrium value p_{crit} despite growth of the imposed basal pore pressure p_i. Negative feedback due to generation of negative excess pore pressure

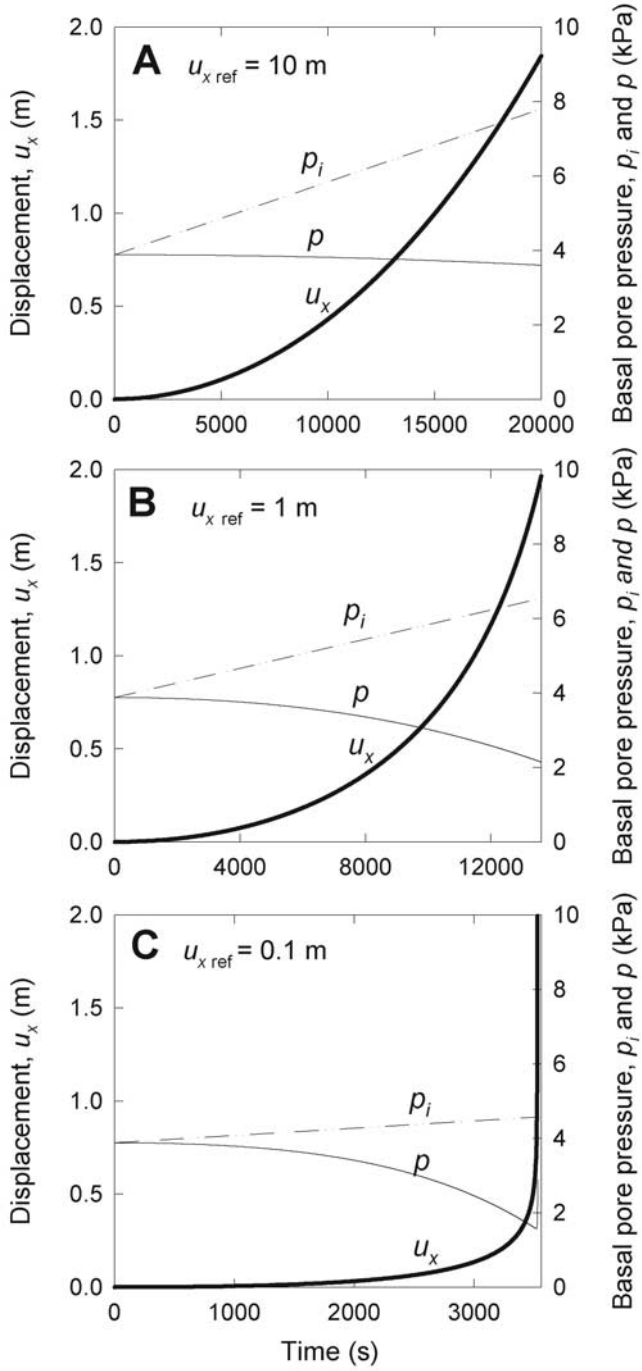

Figure 7. Graphs illustrating the influence of the dilatancy decay constant $u_{x\,ref}$ on evolution of slide block displacement and basal pore pressure computed using parameter values appropriate for landslide experiments with dense loamy sand (Table 1). All computations use $Z = 0.46$ m.

$p_e = p - p_i$ maintains this state, thereby helping to stabilize slide block motion and inhibit rapid acceleration. The existence of this stabilizing effect corroborates analytical inferences described in section 3.

[50] Figures 6a and 6c have time and displacement scales magnified ten times relative to those of Figures 6b and 6d, and comparison of Figures 6a and 6c with Figures 6b and 6d shows that stabilization of slide block motion is greatest during the first ~2000 s. Thereafter, stabilization weakens and slide block acceleration increases as the imposed pore pressure p_i continues to grow.

[51] Figure 7 shows how the behavior depicted in Figure 6d changes if the dilatancy angle ψ decays from its initial value of 6°. The slide block displacement shown in Figure 7a differs only subtly from that shown in Figure 6d because the distance for half-decay of ψ in Figure 7a is large, $u_{x\,ref} = 10$ m. Nonetheless, a slight declining trend in total basal pore pressure is evident in Figure 7a, and this trend accompanies progressive weakening due to decay of ψ. Declining basal pore pressure partially compensates for this weakening, and thereby prevents rapid acceleration of the slide block. However, if the decay distance of ψ is reduced, both slide block acceleration and the attendant decline of basal pore pressure become more prominent (Figures 7b and 7c). Basal pore pressure reduction due to dilation does not keep pace with slide block motion, particularly after displacements exceed the dilatancy decay distance $u_{x\,ref}$.

[52] Figure 7c shows an important feature that appears in all computations with dilatancy decay if the computations are extended to include displacements several times larger than $u_{x\,ref}$. Near the right margin of Figure 7c the total basal pore pressure reaches a minimum and then rises abruptly. The minimum marks the limit of the stabilizing influence of dilatant pore pressure reduction, as thereafter dilation is so slight that negative pore pressure production does not keep pace with the rate of pressure diffusion into the dilating shear zone. This unstable response produces runaway acceleration somewhat analogous to that which accompanies liquefaction (Figure 5b).

4.3. Clay-Rich Landslide With Dilative Soil

[53] Figure 8 depicts graphs analogous to those of Figures 6 and 7, except that the graphs were generated using parameter values appropriate for the clay-rich Minor Creek landslide in northwestern California [*Iverson*, 1984, 1986a, 1986b, 1986c; *Iverson and Major*, 1987]. The Coulomb friction angle, dilatancy angle, and hydraulic conductivity and diffusivity of this landslide all have values significantly smaller than those of loamy sand (Table 1). The thickness H of Minor Creek landslide averages about 6 m, and the wet season water table height Z averages about 5.6 m (i.e., the water table is nearly at the ground surface).

[54] Figure 8a shows baseline results obtained using a constant dilatancy angle, $\psi = 3°$. The small slide block acceleration evident in this graph persists despite the fact that the imposed basal pore pressure increases at nearly the maximum feasible rate. The acceleration is roughly 0.001 times as large as that shown in Figure 6d, and in 7 months it produces a total displacement less than 2 m. The stabilizing influence of dilatancy and pore pressure feedback is very strong in this case owing to the effects of low hydraulic conductivity and diffusivity, which combine to yield a very large value of α (Table 1).

[55] Figures 8b–8d show how behavior changes if the dilatancy angle decays as slide block displacement proceeds. The graphs are qualitatively very similar to those of Figure 7, but in Figures 8b and 8c the slide block accelerations are roughly 0.001 times as large as those shown in Figure 7 for corresponding values of the decay constant, $u_{x\,ref}$. Near the right margin of Figure 8d, the total basal pore pressure p

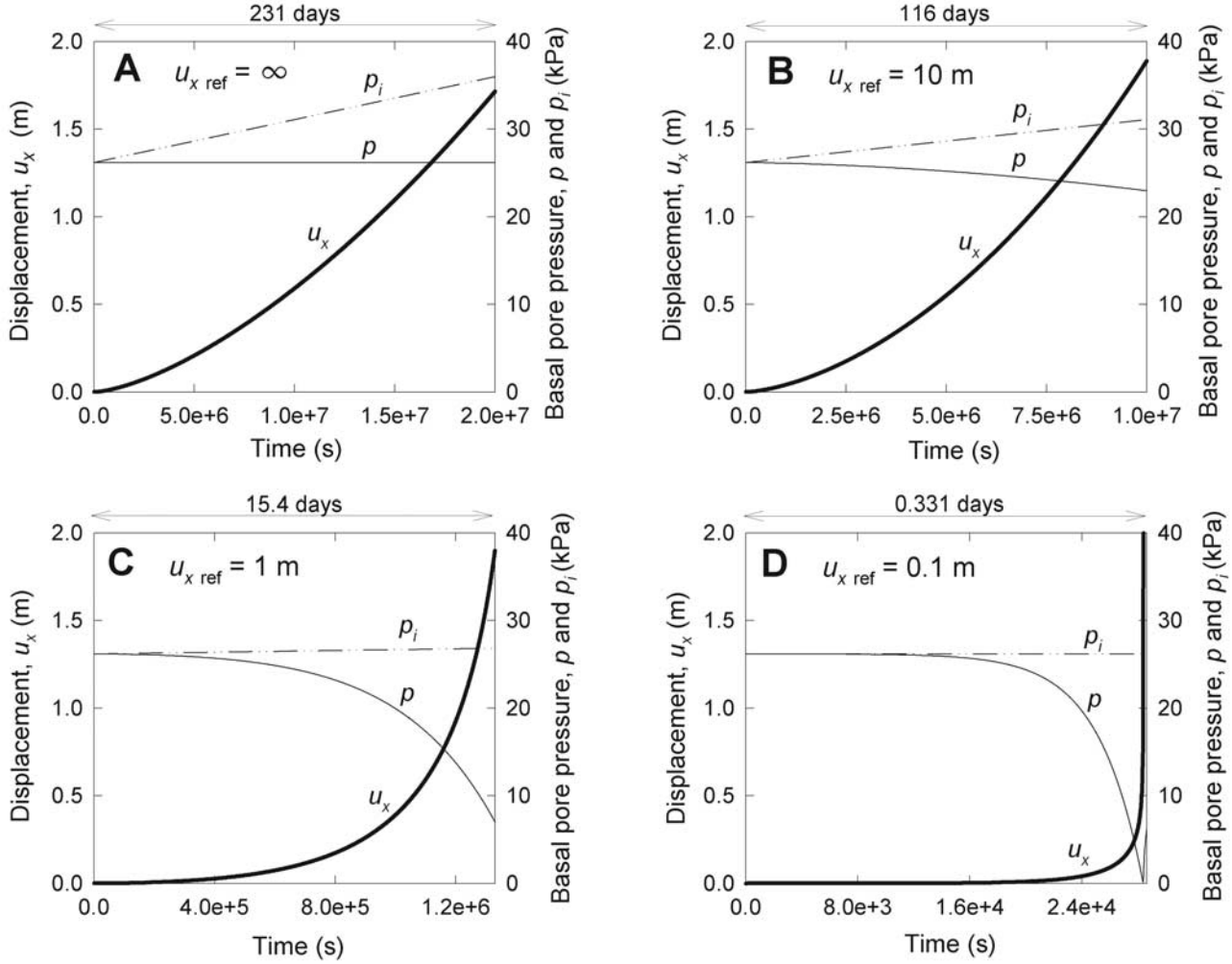

Figure 8. Graphs illustrating the influence of the dilatancy decay constant $u_{x\ ref}$ on evolution of slide block displacement and basal pore pressure computed using parameter values appropriate for Minor Creek landslide (Table 1). All computations use Z = 5.6 m.

exhibits the same type of instability as that shown in Figure 7c, although onset of the instability in Figure 8d is delayed owing to the large value of α. As in Figure 7c, the instability shown in Figure 8d signals the end of stabilization by negative pore pressure feedback.

[56] Figures 9 and 10 compare the measured behavior of Minor Creek landslide with model behavior that occurs in response to transient forcing by seasonal rainfall that causes seasonal changes in imposed basal pore pressure. The model results shown in Figure 9 apply for a constant dilatancy $\psi = 3°$ and use a simple history of imposed basal pore pressure to mimic the effects of seasonal rainfall at Minor Creek landslide. The imposed basal pore pressure p_i increases steadily for 6 months in response to wet season rain infiltration, and then decreases steadily during the ensuing dry season. The initial basal pore pressure is less than the pressure p_{crit} necessary to trigger motion. Thus in Figure 9 landslide motion does not commence until 5×10^6 s (about 58 days) after rainfall commences. Figure 10 shows analogous behavior measured at Minor Creek landslide over a 3 year period in which rainfall and groundwater responses varied somewhat from year to year [*Iverson and Major*, 1987].

[57] The model results and landslide behavior shown in Figures 9 and 10 are similar in several key respects. First, both the model and data indicate a gradual onset of seasonal landslide acceleration followed by prolonged, nearly steady motion and subsequent gradual deceleration. In both the model and data, acceleration commences when basal pore pressures exceed a critical threshold level, and pore pressures do not rise much above this threshold level during the prolonged period of nearly steady landslide motion. The model indicates that modulation of both basal pore pressure and landslide motion is a consequence of shear zone dilation and attendant pore pressure depletion that tends to offset the effect of rain infiltration. The net result is that the landslide tends to move steadily in response to nearly steady basal pore pressure in excess of a critical value – a response that superficially resembles viscoplastic behavior [cf. *Iverson*, 1985].

[58] Taken together, the model's dilatancy angle ($\psi = 3°$) and the downslope displacement shown in Figure 9 ($\sim$0.75 m) imply a total slope-normal displacement of about 4 cm. If the dilatancy angle were reduced, the slope-normal displacement would decline in proportion, as would the amount of negative feedback available to regulate landslide

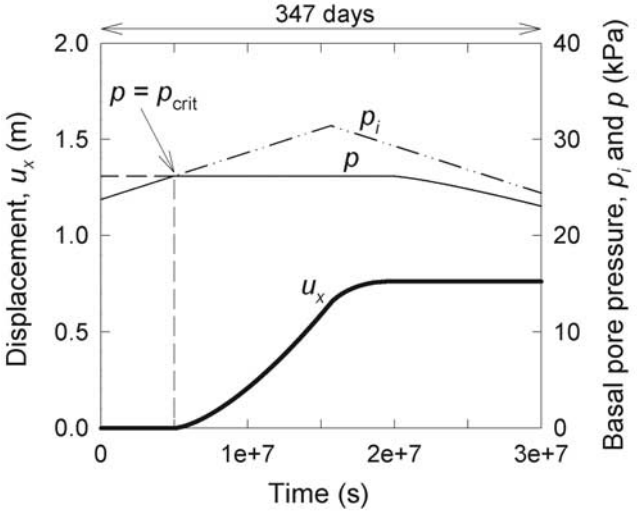

Figure 9. Graph illustrating the computed surface displacement and basal pore water pressure p that occur in response to seasonal changes in the imposed pore water pressure p_i at Minor Creek landslide. Parameter values used in the computations are listed in Table 1.

motion. Thus the model predicts that a few centimeters of wet season uplift of the surface of Minor Creek landslide is required to produce the observed, slow, stabilized motion. Surveys conducted at Minor Creek landslide to date have provided inadequate resolution of slope-normal motion to test this model prediction, but such surveys may be feasible in the future.

5. Concluding Discussion

[59] Landslide motion that is resisted only by Coulomb friction but stabilized by dilatancy and negative pore pressure feedback can bear a strong resemblance to motion resisted by viscous deformation. However, a crucial distinction exists between these modes of motion. Whereas creeping viscous flow is inherently stable with respect to small perturbations, stabilization of motion by dilatancy can be transitory and can evolve into rapid acceleration. Whether or not such a transition occurs depends on both the physical properties of the landslide soil and the history of forcing by rain infiltration. If α values are very large (as is typical for clay-rich landslides) and forcing by rainfall is ephemeral, slow motion might be stabilized permanently by dilatancy and feedback. However, permanently stabilized motion requires that the dilatancy angle ψ does not decay too much during periods of motion, and then recovers to a sufficiently large value during periods of landslide dormancy. Possible mechanisms for dilatancy recovery include dry season soil consolidation and/or dessication. On the other hand, if α values are relatively small (as is typical for sand-rich landslides), stabilization of slow motion is weaker and more transitory. In such circumstances transitions from slow, nearly steady motion to rapid acceleration can occur quickly. If $\alpha < 0$, landslide motion is inherently unstable, and runaway acceleration is inevitable.

[60] Owing to the superficial similarity of inherently stable viscous motion and motion transiently stabilized by dilatancy and pore pressure feedback, field measurements of landslide velocities provide inadequate constraints for understanding or forecasting long-term landslide behavior. However, as noted in section 4.3, high-resolution field measurements of surface elevation change can help determine whether dilation is sufficient to stabilize slow motion. Other key ingredients for such a determination include knowledge of the landslide velocity and the parameters that compose α (equation (28)).

[61] Laboratory studies aid testing of components of the dilatancy feedback model. Detailed monitoring of laboratory landslides with thoroughly characterized soil properties generally supports the importance of coupling between landslide emotion and pore pressure feedback [e.g., *Eckersley*, 1990; *Iverson et al.*, 2000; *Wang and Sassa*, 2003]. However, such studies have been limited to landslides composed of relatively high permeability soil, and traditional laboratory strength testing of clay-rich soil demonstrates the difficulty of generating reproducible results with such material [e.g., *Watry and Ehlig*, 1995]. Understanding of the

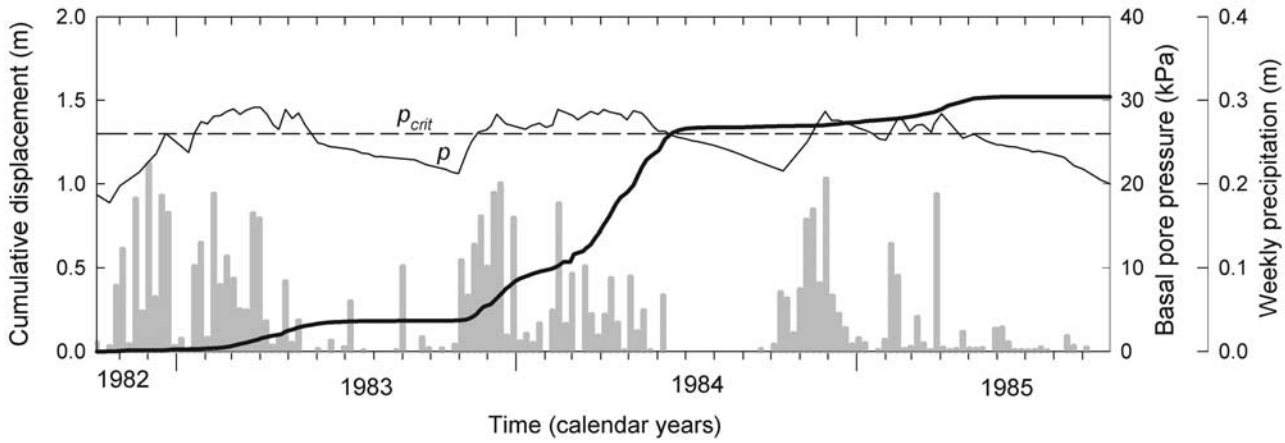

Figure 10. Measured precipitation histogram, basal pore water pressure p, and cumulative surface displacement at Minor Creek landslide during 3 successive water years, beginning 1 October 1982 and ending 30 September 1985 [cf. *Iverson and Major*, 1987]. The critical pore pressure necessary to trigger seasonal motion is p_{crit}.

coupling between dilatancy, pore pressure, and landslide motion may nevertheless be enhanced by laboratory soil testing using nontraditional, stress-controlled apparatus that mimics landslide behavior by permitting unrestricted strain and pore pressure evolution [e.g., *Moore and Iverson*, 2002; *Sassa et al.*, 2004]. Such experiments also help characterize evolution of the dilatancy angle ψ as a function of shear strain, although the problem remains that shear zones in landslides may be much thicker than those in laboratory specimens.

[62] Laboratory experiments can also reveal styles of behavior not represented by the model described here. For example, episodic stick-slip cycles, which appear to be regulated by negative pore pressure feedback, have been observed in both experimental landslides [*Iverson et al.*, 2000] and in ring shear tests [*Moore and Iverson*, 2002], but are not produced by the model. However, similarly episodic motion is predicted by fault models that combine the effects of pore pressure feedback with those of state- and rate-variable friction [*Segall and Rice*, 1995]. Experimental evidence for systematic rate dependence of friction in soils is inconclusive [*Tika et al.*, 1996]. Nonetheless, application of state- and rate-variable friction without pore pressure effects has shown signs of success in explaining some landslide behavior [e.g., *Helmstetter et al.*, 2004]. Investigation of variable friction effects operating in conjunction with pore pressure feedback in landslides therefore appears warranted.

Appendix A: Imposed Pore Pressure Distribution $p_i(z, t)$

[63] This appendix describes how the imposed pore pressure distribution specified by equation (8) represents the effect of transient rain infiltration, while neglecting details of the infiltration process itself. Consider a situation with a preexisting water table positioned at height $z = Z$ above the slide block base at height $z = 0$ (Figure 1). Then, if transient rain infiltration causes the downward slope-normal water influx at $z = Z$ to exceed the slope-normal efflux at $z = 0$, the pore pressure $p_i(z, t)$ at heights $0 \leq z \leq Z$ must increase. Downward water fluxes in the domain $0 \leq z \leq Z$ are assumed to obey Darcy's law, which in this instance has the special form

$$q_z = K[\cos\theta + (1/\rho_w g)\partial p_i/\partial z], \tag{A1}$$

where ρ_w is the pore water density, K is the saturated hydraulic conductivity, θ is the slope angle, and q_z is the specific discharge (volumetric water flux per unit area) in the negative z direction. Generally, this downward discharge is driven mostly by the gravity term $\cos\theta$ but is modulated by the pore pressure gradient $\partial p_i/\partial z$.

[64] To represent an imbalance in q_z between $z = Z$ and $z = 0$, it is convenient to specify the imposed pore pressure gradients at $z = Z$ and $z = 0$ as

$$\frac{\partial p_i}{\partial z}(Z, t) = -\rho_w g\beta \tag{A2}$$

$$\frac{\partial p_i}{\partial z}(0, t) = -\rho_w g(\beta + \gamma). \tag{A3}$$

In (A2) and (A3), β is a dimensionless coefficient (generally $0 \leq \beta \leq 1$) that describes the magnitude of a background, steady state pore pressure gradient $-\rho_w g\beta$ that exists in the absence of a flux imbalance. For the special case with $\beta = \cos\theta$, the steady state gradient is hydrostatic and the downward water flux specified by (A1) is zero. In (A3), γ is a dimensionless coefficient that summarizes the magnitude of a flux imbalance between $z = Z$ and $z = 0$. If $\gamma > 0$, then the downward water flux at $z = Z$ exceeds that at $z = 0$, and the resulting accumulation of water between $z = Z$ and $z = 0$ is accompanied by increased pore pressure. This simple picture of pore pressure change neglects phenomena that occur above height $z = Z$, where pressures may become positive during rain infiltration.

[65] The coefficient γ can be expressed in terms of physical variables by employing some standard definitions used in the theory of saturated porous media. Pressurization of water in a saturated, deformable porous medium is accompanied by volumetric strain (i.e., porosity increase), and the relationship between pressurization and strain can be quantified with varying degrees of sophistication [e.g., *Rice and Cleary*, 1976]. In groundwater hydrology, the relationship between pressurization and strain is commonly summarized in terms of a storage coefficient, which describes the volume of water accumulated within a unit volume of porous medium per unit increase in pressure head, $p_i/\rho_w g$. The storage coefficient S can be expressed in terms of K and D as [*Freeze and Cherry*, 1979, pp. 59–61]

$$S = K/D. \tag{A4}$$

When integrated from $z = 0$ to $z = Z$, S describes the volume of water accumulated within the total thickness of the saturated zone per unit increase in pressure head. That is, for a unit increase in pressure head, the integral

$$\int_0^z S dz = (K/D)Z \tag{A5}$$

provides a nondimensional description of the net water accumulation (or flux imbalance) between $z = Z$ and $z = 0$. The quantity $(K/D)Z$ in (A5) is analogous to the groundwater storativity defined in aquifer hydraulics [*Freeze and Cherry*, 1979, p. 61], and like the storativity, $(K/D)Z$ applies only to fully saturated conditions.

[66] Equation (A5) is easily generalized to address cases in which the change in pressure head differs from a unit change in pressure head by a factor W (where $0 \leq W \leq 2$ is typical). For this arbitrary change in pressure head, (A5) becomes

$$W\int_0^z S dz = W(K/D)Z = \gamma. \tag{A6}$$

This equation defines the relationship between the flux imbalance coefficient γ and the pressure head change factor W. Although γ is used in the lower boundary condition (A3), the substitution $\gamma = W(K/D)Z$ is employed in (11) because it helps reveal the effects of the physical parameters K, D and Z.

[67] The imposed pore pressure distribution ((8) or (12)) is determined by satisfying (10) and (11) along with the governing diffusion equation (9). The intentionally simplistic hydrology represented by this imposed pore pressure distribution is illustrated graphically in Figure 2. Graphs are shown for a typical value of β (0.5) and for the range of $W(K/D)Z$ values most plausible for landslides. For example, $W(K/D)Z \sim 0.1$ applies under conditions prevalent in shallow, high-permeability landslides studied by *Iverson et al.* [2000] and *Montgomery et al.* [2002], whereas $W(K/D)Z \sim 1/3$ applies under conditions prevalent in a thick, clay-rich landslide studied by *Iverson and Major* [1987]. Values of $W(K/D)Z$ as large as 1 would apply only in exceptional circumstances. Figure 2 also depicts graphs of a linearized version of (12) that omits the term $z^*(1 - z^*)$. The correspondence between the linear pressure distributions and exact pressure distributions becomes closer as values of $W(K/D)Z$ decline. This correspondence shows that the transient pressure distributions described by (8) and (12) converge toward a sequence of steady state distributions as W becomes arbitrarily small.

[68] As shown in Figure 2, equations (8) and (12) provide no information about pressure distributions above height $z = Z$, where variably saturated flow and water table accretion may occur. Instead, the equations treat water table accretion as a simple source of pore pressure, and imply that the imposed pressure at $z = Z$ grows with time according to $p_i(Z,t) = \rho_w g W K t$. Although this pressure growth might be used to estimate evolution of the water table height, such estimates are illusory if landslide motion and pore pressure feedback occur, because excess pressure p_e then contributes to regulation of the water table height. Indeed, as shown in sections 3 and 4, in the presence of positive dilatancy a strong tendency exists for excess pore pressure to offset changes in the imposed pore pressure and thereby maintain the water table at a preexisting height Z.

[69] **Acknowledgment.** This work benefited from the input of several people, particularly David Schaeffer, Neal Iverson, Mark Reid, Joseph Walder, and Rex Baum.

References

Baum, R. L., and A. M. Johnson (1993), Steady movement of landslides in fine-grained soils—A model for sliding over an irregular slip surface, *U.S. Geol. Surv. Bull.*, *1842*, 28 pp.

Bolton, M. D. (1986), The strength and dilatancy of sands, *Geotechnique*, *36*, 65–78.

Crank, J. (1975), *The Mathematics of Diffusion*, 2nd ed., 414 pp., Oxford Univ. Press, New York.

Cruden, D. M., and D. J. Varnes (1996), Landslide types and processes, in *Landslides Investigation and Mitigation*, edited by A. K. Turner and R. L. Schuster, pp. 36–75, Natl. Academy of Sci., Washington, D. C.

Denlinger, R. P., and R. M. Iverson (2004), Granular avalanches across irregular three-dimensional terrain: 1. Theory and computation, *J. Geophys. Res.*, *109*, F01014, doi:10.1029/2003JF000085.

Dwight, H. B. (1961), *Tables of Integrals and Other Mathematical Data*, 4th ed., 336 pp., Macmillan, New York.

Eckersley, D. (1990), Instrumented laboratory flowslides, *Geotechnique*, *40*, 489–502.

Frank, F. C. (1965), On dilatancy in relation to seismic sources, *Rev. Geophys.*, *3*, 485–503.

Freeze, R. A., and J. A. Cherry (1979), *Groundwater*, 604 pp., Prentice-Hall, Upper Saddle River, N. J.

Gambolati, G. (1973), Equation for one-dimensional vertical flow of groundwater: 2. Validity range of the diffusion equation, *Water Resour. Res.*, *9*, 1385–1395.

Helmstetter, A., D. Sornette, J.-R. Grasso, J. V. Andersen, S. Gluzman, and V. Pisarenko (2004), Slider block friction model for landslides: Application to Vaiont and La Clapiére landslides, *J. Geophys. Res.*, *109*, B02409, doi:10.1029/2002JB002160.

Hovind, C. L. (1990), Determination of time-dependent soil parameters by triaxial tests, M.S. thesis, 109 pp., Wash. State Univ., Seattle.

Hungr, O. (1995), A model for the runout analysis of rapid flow slides, debris flows, and avalanches, *Can. Geotech. J.*, *32*, 610–623.

Hutchinson, J. N. (1986), A sliding-consolidation model for flow slides, *Can. Geotech. J.*, *23*, 115–126.

Iverson, R. M. (1984), Unsteady, nonuniform landslide motion: Theory and measurement, Ph.D. thesis, 303 pp., Stanford Univ., Calif.

Iverson, R. M. (1985), A constitutive equation for mass-movement behavior, *J. Geol.*, *93*, 143–160.

Iverson, R. M. (1986a), Unsteady, nonuniform landslide motion: 1. Theoretical dynamics and the steady datum state, *J. Geol.*, *94*, 1–15.

Iverson, R. M. (1986b), Unsteady, nonuniform landslide motion: 2. Linearized theory and the kinematics of transient response, *J. Geol.*, *94*, 349–364.

Iverson, R. M. (1986c), Dynamics of slow landslides: A theory for time-dependent behavior, in *Hillslope Processes*, edited by A. D. Abrahams, pp. 297–317, Allen and Unwin, St Leonards, NSW, Australia.

Iverson, R. M. (1991), Sensitivity of stability analyses to groundwater data, in *Proceedings of the Sixth International Symposium on Landslides*, vol. 1, *Landslides*, edited by D. H. Bell, pp. 451–457, A. A. Balkema, Brookfield, Vt.

Iverson, R. M. (1993), Differential equations governing slip-induced pore-pressure fluctuations in a water-saturated granular medium, *Math. Geol.*, *25*, 1073–1094.

Iverson, R. M. (2000), Landslide triggering by rain infiltration, *Water Resour. Res.*, *36*, 1897–1910.

Iverson, R. M., and R. P. Denlinger (2001), Flow of variably fluidized granular masses across three-dimensional terrain: 1. Coulomb mixture theory, *J. Geophys. Res.*, *106*, 537–552.

Iverson, R. M., and J. J. Major (1987), Rainfall, groundwater flow, and seasonal movement at Minor Creek landslide, northwestern California: Physical interpretation of empirical relations, *Geol. Soc. Am. Bull.*, *99*, 579–594.

Iverson, R. M., M. E. Reid, and R. G. LaHusen (1997), Debris-flow mobilization from landslides, *Annu. Rev. Earth Planet. Sci.*, *25*, 85–138.

Iverson, R. M., M. E. Reid, N. R. Iverson, R. G. LaHusen, M. Logan, J. E. Mann, and D. L. Brien (2000), Acute sensitivity of landslide rates to initial soil porosity, *Science*, *290*, 513–516.

Lambe, T. W., and R. V. Whitman (1979), *Soil Mechanics, SI Version*, 553 pp., John Wiley, Hoboken, N. J.

LeVeque, R. J. (2002), *Finite Volume Methods for Hyperbolic Problems*, 558 pp., Cambridge Univ. Press, New York.

Montgomery, D. R., W. E. Dietrich, and J. T. Hefner (2002), Piezometric response in shallow bedrock at CB1: Implications for runoff generation and landsliding, *Water Resour. Res.*, *38*(12), 1274, doi:10.1029/2002WR001429.

Moore, P. L., and N. R. Iverson (2002), Slow episodic shear of granular materials regulated by dilatant strengthening, *Geology*, *30*, 843–846.

Negussey, D., W. K. D. Wijeckreme, and Y. P. Vaid (1988), Constant-volume friction angle of granular materials, *Can. Geotech. J.*, *25*, 50–55.

Nemat-Nasser, S. (1980), On behavior of granular materials in simple shear, *Soils Foundations*, *20*, 59–73.

Press, W. H., B. P. Flannery, S. A. Teukolsy, and W. T. Vettering (1986), *Numerical Recipes*, 818 pp., Cambridge Univ. Press, New York.

Rainville, E. D., and P. E. Bedient (1974), *Elementary Differential Equations*, 5th ed., 511 pp., Macmillan, New York.

Reynolds, O. (1885), On the dilatancy of media composed of rigid particles in contact with experimental illustrations, *Philos. Mag.*, *2*, 469–481.

Reynolds, O. (1886), Dilatancy, *Nature*, *33*, 429–430.

Rice, J. R. (1975), On the stability of dilatant hardening for saturated rock masses, *J. Geophys. Res.*, *80*, 1531–1536.

Rice, J. R., and M. P. Cleary (1976), Some basic stress diffusion solutions for fluid-saturated elastic porous media with compressible constituents, *Rev. Geophys.*, *14*, 227–241.

Roscoe, K. H. (1970), The influence of strains in soil mechanics, *Geotechnique*, *20*, 129–170.

Rowe, P. W. (1962), The stress-dilatancy relation for static equilibrium of an assembly of particles in contact, *Proc. R. Soc. London, Ser. A*, *269*, 500–527.

Rudnicki, J. W. (1984), Effects of dilatant hardening on the development of concentrated shear deformation in fissured rock masses, *J. Geophys. Res.*, *89*, 9259–9270.

Sassa, K., H. Fukuoka, G. Wang, and N. Ishikawa (2004), Undrained dynamic-loading ring-shear apparatus and its application to landslide dynamics, *Landslides*, *1*, 7–19.

Savage, S. B., and R. M. Iverson (2003), Surge dynamics coupled to pore-pressure evolution in debris flows, in *Debris-Flow Hazards Mitigation:*

Mechanics, Prediction, and Assessment, vol. 1, edited by D. Rickenmann and C.-L. Chen, pp. 503–514, Millpress, Rotterdam.

Segall, P., and J. R. Rice (1995), Dilatancy, compaction, and slip instability of a fluid-infiltrated fault, *J. Geophys. Res.*, *100*, 22,155–22,171.

Takahashi, T. (1991), *Debris Flow*, 165 pp., A. A. Balkema, St Leonards, NSW, Australia.

Taylor, D. W. (1948), *Fundamentals of Soil Mechanics*, 700 pp., John Wiley, Hoboken, N. J.

Terzaghi, K. (1943), *Theoretical Soil Mechanics*, 510 pp., John Wiley, Hoboken, N. J.

Tika, T. E., P. R. Vaughn, and L. J. L. J. Lemos (1996), Fast shearing of pre-existing shear zones in soil, *Geotechnique*, *46*, 197–233.

Vulliet, L., and K. Hutter (1988), Continuum model for natural slopes in slow movement, *Geotechnique*, *36*, 199–217.

Wang, G., and K. Sassa (2003), Pore-pressure generation and movement of rainfall-induced landslides: Effects of grain size and fine-particle content, *Eng. Geol.*, *69*, 109–125.

Watry, S. M., and P. L. Ehlig (1995), Effect of test method and procedure on measurements of residual shear strength of bentonite from the Portuguese Bend landslide, *Geol. Soc. Am. Rev. Eng. Geol.*, *10*, 13–38.

R. M. Iverson, U.S. Geological Survey, 1300 SE Cardinal Court #100, Vancouver, WA 98683, USA. (riverson@usgs.gov)